Representativity of the singular stress state in the failure of adhesively bonded joints between metals and composites.

A. Barroso, F. París, V. Mantič

(*abc@esi.us.es*, *paris@esi.us.es*, *mantic@esi.us.es*)

Group of Elasticity and Strength of Materials, Engineering School

University of Seville, Spain

Abstract

Several critical points, where both geometry and material properties change abruptly, arise in an adhesively bonded lap joint between a metallic and a composite material. These critical points, called multimaterial corners or cross-points, at which the linear theory of elasticity predicts unbounded (singular) stresses, are potential points for failure initiation. In this work, a complete stress characterization at these multimaterial corners has been carried out to analyze, after a preliminary experimental test program, the suitability of the application of the parameters defining the singular stress state in the characterization of the failure of these joints. The comparative analysis of the numerical and experimental results obtained show that the singular stress state controlled by a series of the generalized stress intensity factors is controlling the failure path at these corners.

1. Introduction

The massive incorporation of composite materials (in particular plastics with long unidirectional fibre reinforcement) in aeronautic structures raises the need for design methods for the joining process of these materials to the primary part (mainly metallic) of the structure. Two main joining techniques for these metal-to-composite thin-sheet joints are riveting and adhesive bonding. A better behaviour of the adhesive joints under cyclic loads in comparison with the riveted joints, due to a smoother load path transmission, is well known. Nevertheless, the lack of confidence of the manufacturers in using adhesive bonded joints as the only joining technique in primary connections is also known.

This lack of confidence is due, in part, to an insufficient knowledge, first of the complex stress state induced at these multimaterial corners including isotropic (metal and adhesive) and non-isotropic (composite) materials, and second of the complex failure mechanisms characterized by a competition between a sharp crack growth and a plastic or damage zone development in the adhesive layer. There are many different approaches for the stress analysis and for failure criteria proposals used to characterize adhesive joints. They can be roughly divided into several large groups. Historically a first group is represented by the approaches which deal with the nominal stress state obtained in the joint, developing more or less sophisticated failure criteria based on the Strength of Materials Theory. This group includes the classical references by Volkersen [1], Goland and Reissner [2], Hart-Smith [3] and Tsai *et al.* [4]. An understanding of the different models included in this group is in any case highly recommendable, as they illustrate

with greater or lesser complexity the mechanical behaviour of joints of this kind. A second group of approaches deals with the singular stress states induced at the above mentioned multimaterial corners, developing criteria for the failure initiation in the vicinity of these corners controlled by the allowable values of the Generalized Stress Intensity Factors (GSIF), Bogy [5], Bogy and Wang [6], Groth [7], Hattori [8], Leguillon and Siruguet [9], Leguillon *et al.* [10] and Shin *et al.* [11]. Other proposals for the characterization of the failure progress could be roughly grouped into Continuum Damage Mechanics models by Laschet and Stas [12] and Sheppard et al [13], those based on the Plastic or other Non-linear Constitutive Laws for the adhesive layer, e.g. by Crocombe [14], Cohesive-Zone Models for the adhesive layer by Kafkalidis and Thouless [15] and Liljedhal *et al*. [16] and finally the models based on the Interfacial Fracture Mechanics by Malyshev and Salganik [17], Fernlund *et al* [18], Reedy Jr. [19], and Hutchinson and Suo [20].

The present work deals with the failure of the adhesively bonded double-lap joints between Aluminium and CFRP laminates by means of an approach based on the local (singular) stresses, Barroso [21]. Thus, the study is more focused on the onset of the failure than on the progression of the failure itself, which could be further studied by some of the above mentioned models, like the Interfacial Fracture Mechanics or Continuum Damage Mechanics Models. The present work is divided into three parts, the first one dealing with the detailed singular stress characterization at the neighbourhood of the multimaterial corners present in joints of this kind and the second dealing with the experimental determination of the failure load, while the third one

presents an analysis of the two most commonly observed failure paths after testing and their correlation with the previously computed asymptotic singular stress state.

2. Characterization of the singular stress state at the multimaterial corners

The multimaterial corners appearing in an adhesively bonded double-lap joint between a metallic sheet and a composite laminate are depicted in Fig. 1. Consider a polar coordinate system (r, θ) centred at the tip of a corner with the z-axis parallel to the corner front (normal to the section shown in Fig. 1). It is assumed that a generalized plane strain state, with $\varepsilon_{zz}=0$, provides a satisfactory approximation of the stress state at the neighbourhood of the corner except for the free surfaces perpendicular to the corner front. A local stress state at the neighbourhood of the corner tip admits, assuming variable separation and singularities of the type $O(r^{-\delta})$ with $\delta=1-\lambda$ being the order of stress singularity, the following series expansion representation:

$$
\begin{aligned}
\sigma_{ij}(r,\theta) &\cong \sum_{k=1}^{n} \frac{K_k}{r^{1-\lambda_k}} f_{ijk}(\theta) \\
u_i(r,\theta) &\cong \sum_{k=1}^{n} K_k r^{\lambda_k} g_{ik}(\theta)
\end{aligned}
\qquad (i,j=r,\theta,z) \qquad (1)
$$

The terms in (1) with $\delta>0$ are called singular, as they represent unbounded stresses as $r \to 0_+$. The rigid body motions are included in (1) for $\lambda=0$ and $\lambda=1$ with the appropriate definition of g_{ik} and f_{ijk}. The characteristic functions $f_{ijk}(\theta)$ and $g_{ik}(\theta)$ together with the characteristic exponents λ_k only depend on the local geometry and material properties and the type of local boundary conditions prescribed along the corner edges. The constant weights K_k of the terms in (1), called Generalized Stress Intensity Factors (GSIF), are associated to each specific stress state defined at the corner tip and depend

on the global boundary conditions prescribed, and in particular they are proportional to the load magnitude.
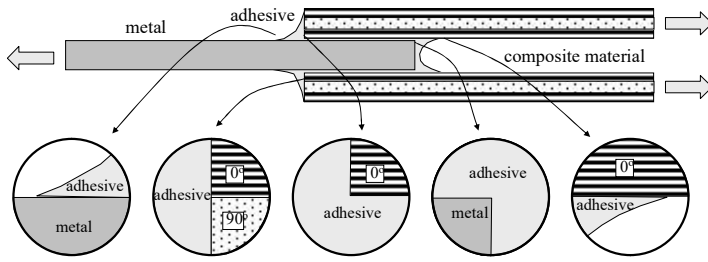

Fig 1. Multimaterial corners appearing in a metal-to-composite double-lap joint.

The equivalent thermo-elastic properties for the carbon/epoxy unidirectional lamina (AS4/8552), modelled like an orthotropic material, are E_{11}=141.3 GPa, E_{22}=E_{33}=9.58 GPa, G_{12}=G_{13}=5.0 GPa, G_{23}=3.5 GPa, v_{12}=v_{13}=0.3, v_{23}=0.32, α_1=-1·10^{-6} ºC^{-1}, α_2=α_3=26·10^{-6} ºC^{-1}, whereas the isotropic elastic properties of the adhesive and aluminium, respectively, are E=3.0 GPa, v=0.35, α=-45·10^{-6} ºC^{-1} and E=68.67 GPa, v=0.33, α_1=-24.5·10^{-6} ºC^{-1}. The curing temperature of the adhesive is 120ºC, so a ΔT=-95ºC is considered for the analysis (the room temperature is 25ºC).

The semianalytic evaluation of λ_k, $f_{ijk}(\theta)$ and $g_{ik}(\theta)$ has been carried out using the computational tool developed by Barroso *et al.* [22]. For each corner shown in Fig. 1, the values of a few first characteristic exponents λ_k obtained are shown in Table 1, omitting those associated to rigid body motions. For each corner, the characteristic exponents which give rise to singular terms (λ_k<1 and δ>0) and the first regular (non-singular) term have been computed. The characteristic exponents of the antiplane singular modes (λ_a), which will not appear in the particular configurations studied in the

present work (due to the geometry, material constitutive laws and loading conditions of the problems), have also been computed and are shown, for the sake of completeness, in Table 1.
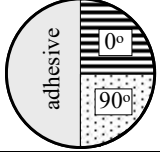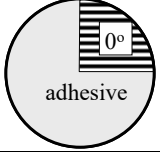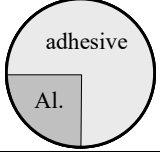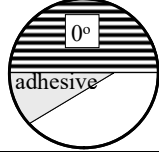

λ_1=0.986914 λ_a=0.994223 λ_2=1.926197	λ_1=0.901497 λ_2=1.01447	λ_1=0.763236 λ_a=0.813696 λ_2=0.889389 λ_3=1.106980	λ_1=0.686272 λ_2=0.696605 λ_3=0.791014 λ_4=1.152813	λ_1=0.905312 λ_a=0.971021 λ_2=1.700273

Table 1. Characteristic exponents for the multimaterial corners.

The GSIFs K_k corresponding to two particular double-lap joint configurations have been evaluated by means of the Boundary Element Method (BEM), París and Cañas [23] and Graciani [24], together with a simple and robust procedure based on a least squares adjustment, developed by Barroso *et al.* [25].The least squares adjustment procedure is based on the minimization of the error between the numerical solution (by BEM) and the analytical one (1) in which the K_k (k=1,...,n) are the unique unknowns. The squares if differences in nodal displacements (2) and in the nodal stress vectors (3) at the boundaries are summed together in (4), N_θ and N_r in (2-3) denoting respectively the number of components, the radial edges to be taken into account and the number of nodes taken at different radial distances.

$$J_u = \sum_{\alpha=r,\theta} \sum_{i=1}^{N_r} \sum_{j=1}^{N_\theta} \left[u_\alpha^{BEM}(r_i,\theta_j) - u_\alpha^{series}(r_i,\theta_j,K_1,...,K_n) \right]^2 \tag{2}$$

$$J_t = \sum_{\alpha=r,\theta} \sum_{i=1}^{N_r} \sum_{j=1}^{N_\theta} \left[T_\alpha^{BEM}(r_i,\theta_j) - T_\alpha^{series}(r_i,\theta_j,K_1,...,K_n) \right]^2 \tag{3}$$

$$J(K_1,...,K_n) = aJ_u + bJ_t \qquad (a,b \geq 0) \qquad (4)$$

A set of K_k (k=1,...,n) which minimizes J in (4) is obtained by solving the following linear system of equations:

$$\frac{\partial J(K_1,...,K_n)}{\partial K_k} = 0, \quad (k\text{=}1,...,n) \qquad (5)$$

The schemes of the double-lap joints analyzed in this work are shown in Fig. 2, where, due to the symmetry, only half of the problem geometries are modelled. The right-hand end of the laminate is fixed while the left-hand end of the aluminium sheet has a uniform tensile stress of 125 MPa. The two configurations analyzed differ in the composite adherent, the first including a unidirectional laminate $[0]_8$ and the second a cross-ply laminate $[0_2/90_2]_s$.

The computed values of the GSIFs K_k corresponding to three corners from the five shown in Fig. 1 and associated to the characteristic exponents λ_k shown in Table 1 (except for λ_a) are presented in Table 2. These corners have been chosen because of the positive peel stress appearing at the adhesive layer at this extreme of the overlap zone.
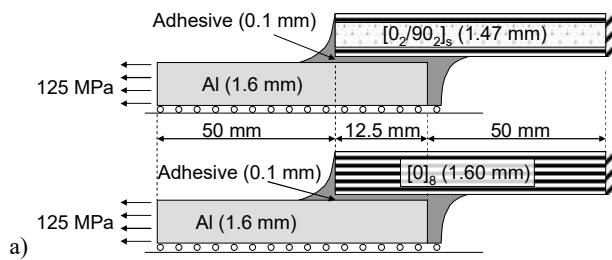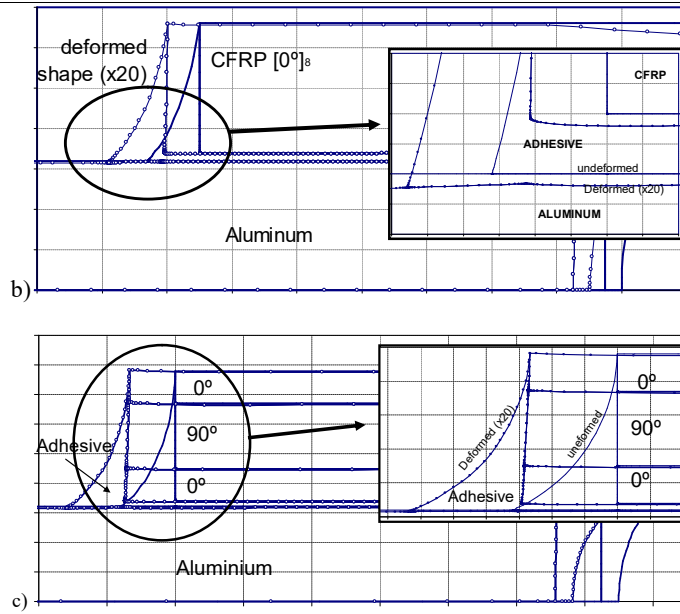
Fig. 2. a) Double-lap joint configurations and BEM models: b) AL-$[0]_8$,c) Al-$[0_2/90_2]_s$.

The dimensions of K_k, standardized following Pageau *et al.* [26], depend on the value

of the associated characteristic exponent (λ_k), the units being (MPa·mm$^\delta$). The values of

K_k have been normalized taking $f_{\theta\theta k}(\theta = 0) = 1$, where $f_{\theta\theta k}(\theta)$ are the characteristic

functions appearing in the series expansion (1) of the circumferential stress $\sigma_{\theta\theta}(r,\theta)$.

The asymptotic series expansion of stresses and displacements in (1), when including

the two singular terms and the first regular term, have been shown to fit accurately the

numerical results obtained by the BEM model at points inside the adhesive. As an

example, Fig. 3 shows the values of the circumferential stress component $\sigma_{\theta\theta}$, for

corner #1 (Table 2) in the adhesive joint Al / $[0]_8$ and at a distance r=0.019 mm from the

corner tip, computed by the BEM model (circles) and by the asymptotic series

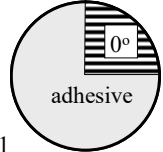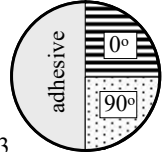expansion (1) considering 1, 2 and 3 terms of this series (continuous lines).

	1	2	3
Al / $[0]_8$	K_1= -0.00275036 K_2= 0.0273839 K_3= -0.0114328	K_1= 0.000723935 K_2= 0.000313232	
Al / $[0_2/90_2]_s$	K_1= -0.00253126 K_2= 0.0225756 K_3= -0.0100326	K_1= 0.00088457 K_2= 0.00017434	K_1= 0.00357711 K_2= 0.00188352

Table 2. Generalized Stress Intensity Factors K_i [MPa·mm$^\delta$] for the corners analyzed.

From Fig. 3 we can observe that, despite the small distance to the corner tip considered,

neither the most singular term (Term 1) alone nor the two singular terms (Term 1 +

Term 2) are able to accurately fit the BEM results at the internal points. Only when the

first regular (non-singular) term is included in the asymptotic series representation

(namely Term 1 + Term 2 + Term 3) is a good fitting of the BEM results achieved. As

all the observed failures run through corner #1, the analyses have also been focused on

this corner. The local maximum values of the σ_θ stress component (for θ=120º and

θ=315º) are located inside the adhesive wedge (90º<θ<360º). The boundary conditions

applied are those depicted in Fig. 2a, with fixed displacements at the right hand side of

the CFRP laminate, symmetry conditions at the bottom sides of the aluminium plate and

adhesive fillet, and a constant tensile value of 125 MPa at the left hand side of the
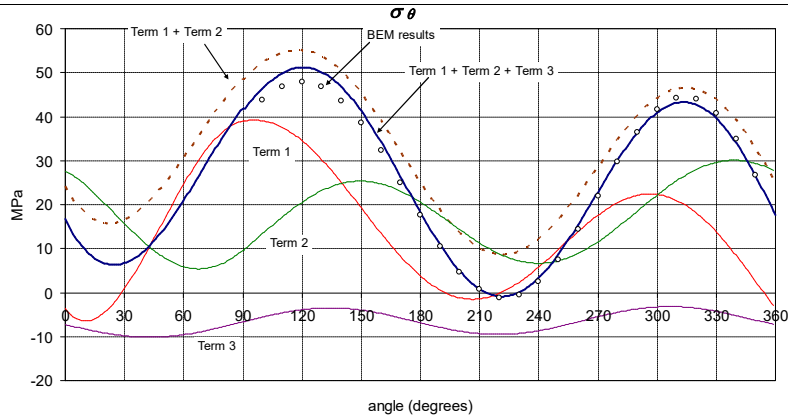
aluminium plate.

Fig. 3. Comparison of σ_θ computed by the asymptotic series expansion and the BEM at points inside the adhesive (corner #1 in the Al/[0]$_8$ configuration).

Taking into account the characteristic length for the heterogeneity of a composite lamina, given by the fibre diameter 5~7 μm, it can be expected that the results for elastic fields obtained inside the adhesive by considering an equivalent homogenized orthotropic lamina will be representative over distances larger than a few (at least two or three) fibre diameters. Thus, in the real adhesive joint the distance r=0.019 mm from the corner tip of a point inside the adhesive is just at the limit below which the heterogeneity of the laminate would affect the representativity of the stress state calculated using the homogeneity assumption. Notice that this distance is about 20% of the adhesive thickness between the laminate and the aluminium. A similar comparison between BEM and asymptotic series expansion results has also been performed at closer distances to the notch tip (r=0.0017 mm), although the representativity is, in mechanical terms, meaningless (as the distance is less than a single fibre diameter), simply to verify

the number of terms which have to be included for a reasonable fitting of the BEM

results, finding that again the three terms had to be included for a satisfactory

agreement.

3. Experimental testing of metal to composite adhesive joints

The two configurations shown in Fig. 2 were bonded in a hot press plate using a film

adhesive (CYTEC FM-73M.06) by means of the curing cycle recommended by the

adhesive manufacturer. The double-lap joint samples with metallic and composite

adherents were mechanized using a vertical saw for the metallic part and a water cooled

diamond disc for the composite, with a final lateral sanding to obtain the final

dimensions of the samples and to eliminate the surface roughness, always avoiding

excessive heating of the samples. Two different surface treatments in the aluminium

sheet were used: anodized and scaled. The samples were tested in a universal testing

machine (Fig. 4) following the requirements of the ASTM D3528 [27] for double-lap

joints in tension.

Fig. 4 - Testing of the samples in shear by a tensile loading.

Fig. 5 shows three of the load-displacement diagrams obtained. The displacement in

Fig. 5 was measured using the cross-head displacement. The load-displacement diagram

shows a stiffening behaviour which is associated to the clamping system and to the

chosen variables. The difficulty in finding a representative definition of the strain has made it preferable to use the *F-u* representation. Additionally, some of the tests were carried out using an extensometer (L_o=25 mm) covering the overlap zone, to evaluate the overlap zone load-displacement behaviour. In both cases, no significantly large yielding effects were observed in the final part of the load displacement curves.
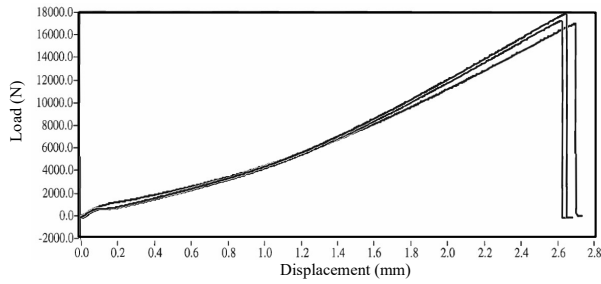

Fig. 5 - Force-displacement diagram of the tests.

From the tests, the apparent shear strength has been obtained dividing the ultimate load by the overlap bond area: $\tau_R(\text{MPa})=F(\text{N})/A_{overlap}(\text{mm}^2)$. In Table 3, the experimental test results are summarized, A and S (in the third column) denote respectively anodized (A) and scaled (S) surface treatments for the aluminium sheet, the standard deviation and the variation coefficient (VC) also being included.

Configuration	$L_{overlap}$ (mm)	Al. (Surf. treatment)	τ_R (MPa)	Std. Dev. (MPa)	VC (%)	nº of tests
1a) Al(3.2 mm)-$[0]_8$	12.5	A	22.26	0.65	2.94	5
1b) Al(3.2 mm)-$[0]_8$	12.5	S	22.03	1.04	4.73	5
2a) Al(3.2 mm)-$[0_2/90_2]_s$	12.5	A	25.01	1.20	4.81	5
2b) Al(3.2 mm)-$[0_2/90_2]_s$	12.5	S	25.56	2.13	8.35	5

Table 3. Experimental test results.

As can be observed in Table 3, no significant influence of the surface treatment on the apparent shear strength is observed for these static tests.

Once the mean failure load was experimentally evaluated, partial load tests (up to 90% of the mean failure load) were also carried out, and then polished, to check (using optical microscopy) whether any damage close to the corner tip was observed before the catastrophic failure. The picture in Figure 6 corresponds to the mid-plane of the sample in order to be fully representative of the generalized plain strain field, which has been assumed in the analysis. Additionally, it has been checked numerically that the edge effects generating a three-dimensional stress state appear only near the free edge and have a significant influence only at a distance of the order of one or two times the adherent thickness inside the sample. No damage was observed, as can be seen from Fig. 6.
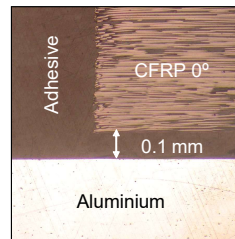
Fig. 6. Corner #1 in Al-$[0]_8$ inspected (at the mid-plane) after a partial (90%) loading.

This fact, together with the evidence of the Force-Displacement diagram (Fig. 5) leads to the consideration that, using this particular configuration, materials and type of loading, the initiation of damage at the corners and the final catastrophic failure of the joint are events which happen close in time. No significant failure progression phenomenon was detected before the final failure.

4. Failure analysis at the multimaterial corners

From the above described tests, different failure paths have been observed in each configuration. Two particular failure paths, one at each configuration, will be analyzed in detail in Sections 4.1 and 4.2 following. For both, the maximum circumferential stress has been used as the criterion to predict the failure orientation, which is a common approach often assumed in situations similar to the one considered here.

4.1. Failure path in aluminium - unidirectional composite [0] $_8$ samples

The most commonly observed failure path in these joints is shown in Fig. 7, only a few samples being observed to fail with a crack running along the vertical adhesive-laminate interface. The failure goes from the corner at the end of the laminate in contact with the adhesive fillet (corner #1 in Table 2) and runs inside the adhesive fillet at an angle between 29º and 33º (for the tested coupons) measured counterclockwise from the adhesive-composite vertical interface (32º for the sample in Fig.7 in particular). The inspection of the failure path (Fig. 7) seems to confirm that the adopted maximum circumferential stress criterion is a reasonable failure criterion as the failure path runs in the radial direction from the corner tip associated to the $\sigma_{\theta\theta}$ stress component. The left-hand side of Fig. 7 shows the picture after failure, while the right-hand side shows the same picture adding the boundaries of the three different materials and the failure path, to help the observation of the failure.
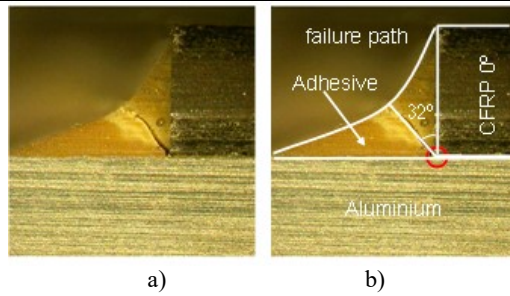
Fig. 7. Failure path in the Al-CFRP[0]$_8$ configuration.

As mentioned previously, only a few samples have shown a failure path running along the adhesive-laminate vertical interface, this alternative failure being due to a poor bonding associated to the procedure followed. The failure pattern running inside the adhesive fillet was found in almost all samples with slightly different angle values, some of which are shown in Fig.8. The average failure angle, measured from the vertical interface was 30.5º with a variation coefficient of 6%.

Fig. 8. Failure angle variation in the Al-CFRP[0]$_8$ configuration.

Once the capability of the series expansion to fit the numerical data (Fig. 3) is demonstrated, and for the sake of simplicity, Fig. 9 shows the stress distribution obtained by BEM of the asymptotic stress state at corner #1 in the Al-[0]$_8$ configuration

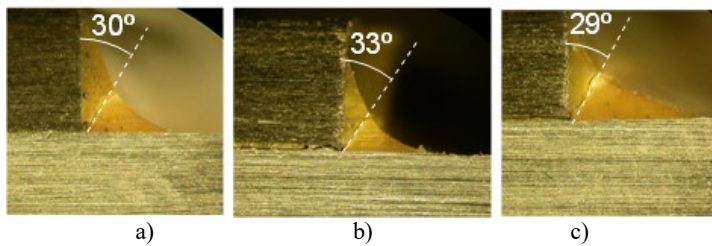at r=0.019 mm, with a diagram (left-hand side of Fig. 9) showing the polar distribution

of σ_θ component (the circumference with dots giving the zero reference value, with

positive values of σ_θ being outside this circumference). The right-hand side of Fig. 9

shows all the stress component variation inside the adhesive wedge (90º<θ<360º).

When taking into account the results for the circumferential stress component (Fig. 3 for

the detailed contribution of each term of the asymptotic series expansion of σ_θ and Fig.

9 for all the stress components), the failure path predicted by the sole contribution of the

most singular term of σ_θ (Term 1) could be expected to occur at an angle $\theta \cong 97^o$ (7º

measured counterclockwise from the vertical interface). The geometry, loading and

boundary conditions are those depicted in Fig. 2, corresponding to the Al-$[0_2/90_2]_s$
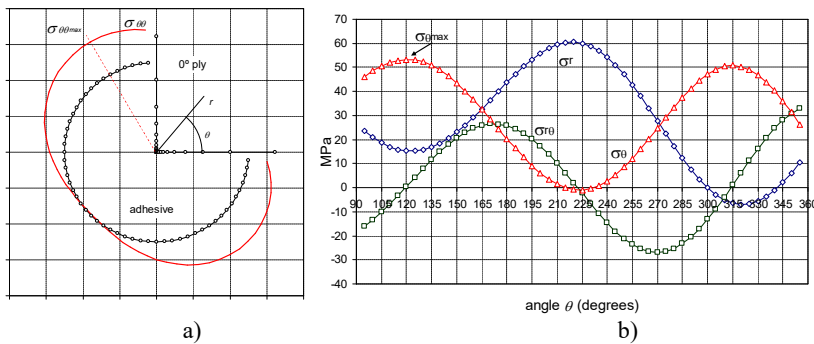
configuration.

Fig. 9. Stresses inside the adhesive at corner #1 in Al-CFRP$[0]_8$ configuration

a) polar plot of σ_θ, b) angular dependence of σ_θ, σ_r, $\sigma_{r\theta}$.

Taking the first two singular terms together (Term 1 + Term 2) would increase the

failure angle predicted up to $\theta \cong 118^o$ (Fig. 3). It should be stressed here that, according

to a discussion in Section 2, these two singular terms dominate the local elastic stress state only at distances from the crack tip below the representativity limit-length associated to the heterogeneous character of a unidirectional lamina, given by at least a few fibre diameters (say about 20μm). Once the contribution of the first regular term is added to the two singular terms (Term 1 + Term 2 + Term 3), which is sufficient to fit very well the numerical results from BEM at the distance given by the representativity limit-length (see Fig. 3 and Fig. 9), the failure angle predicted is about $\theta \cong 120^{o}$ (30º measured counterclockwise from the vertical interface, the angle which is plotted in Fig. 9), showing an excellent agreement with the experimental evidence.

Let us note the fact that in Fig.9 σ_r has higher values at $\theta \approx 215º$ than σ_θ at $\theta \approx 120º$. Assuming that this stress state is controlling the failure orientation at the initiation stage, both failure criteria, the one associated to maximum values of σ_θ and the one associated to maximum values of σ_r, would give the same orientation of the initial crack as both stress components have their maximum values separated approximately 90º from each other. The propagation stage of the initial failure, observed in the macroscopic failure path, is governed by the σ_θ component as the maximum σ_θ orientation remains approximately the same along the observed failure path.

4.2. Failure path in aluminium - cross-ply composite [0₂/90₂]ₛ samples

In the Al-CFRP[0/90]s configuration, three different failure paths were observed:

a) The first one (Fig. 10a) qualitatively and quantitatively similar to the one analyzed in Section 4.1, with the failure path going from the 0º-adhesive bimaterial corner into the

adhesive fillet, so that the observed failure angle, approximately 30º, measured from the vertical interface, is in agreement with the comments in Section 4.1. This is the most often observed failure path, in approximately 80% of the samples. This case was fully studied in Section 4.1 and therefore will not be analyzed again.

b) Another failure path (Fig. 10b) running along the laminate-adhesive vertical interface, which can be favoured by a low quality of the interface bonding (let us remember the lack of hydrostatic pressure when curing in the hot plate press). This failure path was observed in approximately 10% of the samples, most of them having a large adhesive fillet.

c) A third failure path (Fig. 10c), initially observed running along the vertical interface of the 0º layer and the adhesive fillet, and then kinking inside the adhesive fillet. This failure was also observed in approximately 10% of the samples, but is the most challenging from a case-study point of view, as the original failure path is affected by the presence of a three-material corner whose presence changes its original direction. This is the reason why this failure is analyzed in detail in what follows. Slightly different angles were observed inside the adhesive fillet, having an average value (measured from the vertical interface) of 48.5º and a variation coefficient of 12.8%.
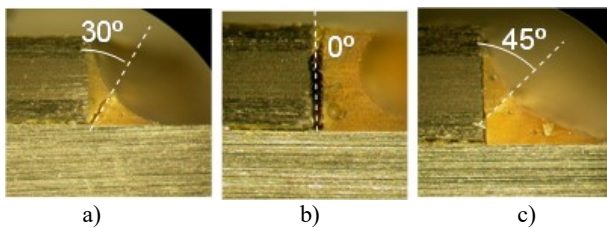

Fig. 10. Failure angles and paths in the Al-CFRP[0/90]s configuration.

The activation of a particular failure path depends on the quality of the interface bonding, the aim of this work not being to predict one of them, but to study them. The third failure path was, from the authors' point of view, the most interesting as the stress state changes qualitatively as the failure progresses and there is a challenge in correlating the failure angle inside the adhesive fillet with the analytical and numerical predictions.

The analyzed failure path for the Al-$[0_2/90_2]_s$ configuration (shown in Fig.11) starts at the bottom multimaterial corner of the laminate, which is locally equivalent to the corner studied in Section 4.1 (corner #1 in Table 2), with a 0º ply in contact with the adhesive, and runs along the vertical interface between the adhesive and the 0º ply. When this interface crack reaches the three-material corner formed by the two unidirectional laminas 0º and 90º and the adhesive fillet (corner #3 in Table 2), both the stress state and the interfacial strength change, this fact resulting, in some of the observed cases, in a kink of the failure path into the adhesive fillet at an angle of approximately 45º measured counterclockwise from the vertical interface. The left-hand side of Fig. 11 shows the picture after failure, while the right-hand side shows the same picture adding the boundaries of the different materials and the failure path.
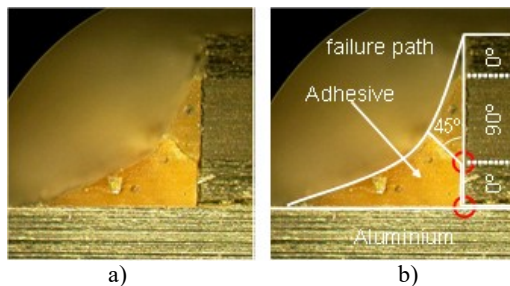

a)   b)

Fig. 11. Failure path in the Al-CFRP$[0_2/90_2]_s$ configuration.

The singular stress state in the undamaged situation at the bottom bimaterial corner is qualitatively and quantitatively similar to that previously studied for the Al-CFRP[0]$_8$ configuration in Fig 9. As materials and geometry at the bottom corner tip are locally the same in both double-lap joints, the characteristic exponents λ_k (presented in Table 1) and the characteristic functions $f_{ijk}(\theta)$ coincide as well. Only the GSIFs K_k associated to this corner change slightly between the two double-lap joints, see results for corner #1 in Table 2. The existence of a three-material corner in this double-lap joint configuration makes it necessary to analyze the stress state at the undamaged three-material corner, in order to compare it with the stress state at the bimaterial bottom corner and to assess the locus of the initiation of failure.

The distribution of stresses at a distance r=0.019 mm from the undamaged three-material corner is shown in Fig. 12, which similarly to Fig. 9 shows the polar variation of σ_θ at the left-hand side of the figure and all the stress components at the right-hand side of the figure. Comparing the stress state in Fig. 12 with the stress state at the undamaged bimaterial corner (see Fig. 9), a significantly lower level of the maximum values of σ_θ at the three-material corner can be observed. Then, if the onset of the failure in the form of a crack running through the adhesive fillet is governed by the maximum circumferential stress criterion, this failure is predicted to start at the bottom bimaterial corner (corner #1 in Table 2).
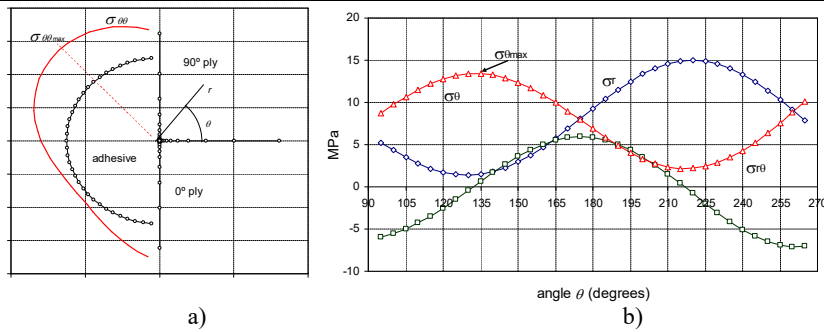
Fig. 12. Stress state inside the adhesive at the undamaged three-material corner,

a) polar plot of σ_θ, b) angular dependence of σ_θ, σ_r, $\sigma_{r\theta}$.

Consider now the other observed failure path including a debonding between the adhesive and the lateral edge of the bottom 0º lamina. The σ_θ stress values along the vertical interface in the undamaged configuration is quantitatively similar (see Fig. 9) to the maximum value (at an angle of 30º measured counterclockwise from this vertical interface), and therefore the relative values of the bulk adhesive strength and the interfacial strength are decisive for the crack path progression in one or the other direction. It is important to stress that these samples have been cured using a hot plate press in which the pressure is only acting in the thickness direction, with no pressure on the adhesive fillet (which is present when using an autoclave and a vacuum bag). Thus, the lack of pressure during the bonding stage can seriously affect the quality of the bonding in this lateral face (the lateral edge of the laminate in contact with the adhesive fillet).

Assuming an initial failure running along this vertical interface, once the interface crack reaches the three-material corner, not only the stress state at this corner has changed (in

comparison with the previous undamaged situation), but the interfacial strength ahead of the crack has also changed, as the fibre orientation in the adjacent lamina is 90º instead of 0º in the bottom lamina. It is then necessary to analyze the altered stress state of the damaged configuration, in which a debonding failure between the lateral edge of the 0º lamina and the adhesive fillet is considered.

The modified stress state at the damaged three-material corner (r=0.019 mm) is shown in Fig. 13 (showing, in a similar way to the previous cases, the polar variation of σ_θ inside the adhesive at the left-hand side of the figure and all the stress components at the right-hand side). The maximum values of the σ_θ stress now occur at an angle $\theta \cong 135^\circ$ (45º measured counterclockwise from the vertical interface) and the stress level is now similar to that associated to the failure onset at the bottom corner (Fig. 9).
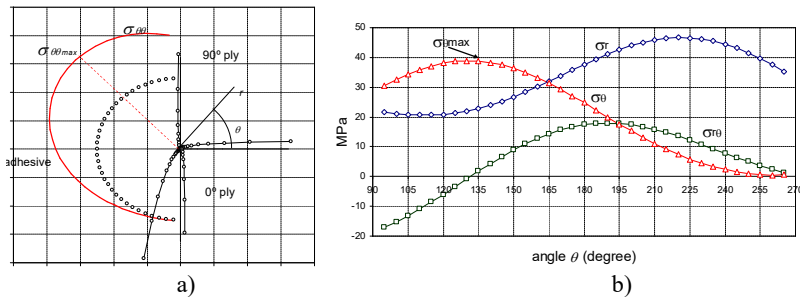
Fig. 13. Stress state inside the adhesive at the damaged three-material corner,

a) polar plot of σ_θ, b) angular dependence of σ_θ, σ_r, $\sigma_{r\theta}$.

Thus, it can be fully justified that the failure can start at the bottom bimaterial corner and grow along the vertical interface between the 0º lamina and the adhesive fillet, and once the failure reaches the three-material corner, the stress state level for σ_θ is high

enough for the crack to kink into the adhesive, the predicted failure angle being in excellent agreement with the experimental evidence.

In any case, the previous analyses of the alternative failure paths require, if they are to be predicted in advance, not only the values of the stresses but also the values of the interface strength/toughness of all the different interfaces and bulk adhesive, which is not an easy task in all cases. The aim of this *a-posteriori* analysis is simply to check the suitability of the tool developed to justify the experimentally observed failure paths. At this early stage of the work, the tool developed is not aimed to be used in a design procedure, but gives the designer a great deal of information regarding the stress state at these corners, not only the stress values, which can be evaluated by means of any conventional numerical analysis, but also the decomposition of these stresses in singular and regular terms, which can be of great help in the understanding of failure mechanisms associated to individual singular terms or a combination of them.

5. Discussions

The fact that the direction of crack propagation presents a good agreement with the predictions obtained from standard BEM analysis (using regular elements without special shape functions, though using a very refined mesh suitable to take into consideration the presence of a singular field), might be misleading as regards the real value and the representativity of the research carried out. The following reasonings represent an attempt to clarify these questions.

First of all, two types of analysis have been carried out: one numerical and the other based on an analytical study of the singular stress state at the corner. To obtain similar results by means of both approaches is a necessary condition to initiate any analysis derived from these results, due to the risk of getting non-accurate results by one or both of these approaches.

In this sense, numerical results in presence of a singularity may be wrong if an appropriate mesh is not used. For instance, in the case considered and for the mesh used, if an attempt is made to calculate displacements or stresses at points closer to the corner , the results will start to be contaminated at some distance by the presence of the singular modes.

The results derived from an asymptotic series expansion are obtained after an elaborate procedure involving analytical developments and numerical calculation that might also involve mistakes. But even having done everything to avoid mistakes, the number of terms used might simply not be representative at the distance taken to perform the comparison.

The coincidence of the results predicted by the BEM analysis (which does not take into consideration the singular nature of the stress state) and the series expansion results (which do) gives full confidence in each of the procedures followed, although this coincidence is not an objective of the paper, but a requirement.

Now, entering into the comparison of the two procedures, it has to be pointed out that this comparison is performed at a distance of 20 micrometers (of an order of 2 or 3 fibre diameters), a distance that can be representative of the mechanical phenomenon of generation and appearance of the damage in absence of initial cracks. To see what happens in terms of stresses either at or along a certain representative distance to the potential point of appearance of damage (the corner tip in this case) is a classical approach, see for instance the transcendental work of Wieghardt [28] (1907, republished in English in 1995), the proposals by Whitney and Nuismer [29] and many others being reviewed in Taylor [30].

Thus, with reference to the corner between the 0º layer and the adhesive (Fig. 2), three terms of the series expansion are, at this distance, sufficient to obtain a solution coincident with that obtained by BEM. Two of these terms correspond to the presence of weak singularities and only the third corresponds to a non-singular term. The weight of the non-singular term in the solution is only about 6 % of the total stress, which proves that the terms corresponding to the weak singularities associated to the corner control the stress state at the distance considered representative of the initiation of the damage.

Now, if the analysis of the singularities carried out in this paper had not been performed, and having only the results associated to BEM, which moreover predict correctly the direction of propagation of the crack, one might think that the value of the stresses (the circumferential stress in this case) controls the initiation of damage in absence of a previous crack. The development carried out in this paper, by contrast, points to a

different parameter. Considering that the difference between the total stress and that originated by the singular terms is only in the order of 6%, it becomes necessary to clarify whether the generalized stress intensity factors associated to these two terms are governing the initiation of the damage.

The knowledge of singular stress fields has also afforded a support to explain more complicated damage morphology. Thus, in the case of $[0,90]_s$ laminates, two corners appear to be involved, Fig. 11, in the observed damage. The singular stress states that appear at both corners (in the first corner in absence of cracks and in the second in presence of the crack that started at the first corner) have given a plausible and coherent explanation of the path followed by the crack.

All this is the actual value of the analysis carried out. The fact that the propagation direction predicted by a regular (very fine, but regular) BEM analysis coincides with that predicted by a singular analysis, and both with that found experimentally, can not hide the potential that knowledge of the singular stress state controlled by generalized stress intensity factors may have for the prediction of the behaviour of adhesively bonded joints.

The question concerning the role of these generalized stress intensity factors is still open and necessarily has to be clarified by means of suitable tests able to prove their representativity. These tests must also provide the joint material characteristics

(allowable values in terms of strength and/or toughness of interfaces) to enable the approach to have predictive capabilities.

Two final questions can be mentioned to conclude this discussion. One is the possibility that neither the stresses nor the generalized stress intensity factors independently control the appearance of the damage. A coupled criterion based on the singular stress state and energy released by a potential crack might play this role, as proposed for instance by Leguillon and co-workers [9, 10, 31] and Cornetti et al [32].

The second question is that the elastic analysis carried out is only valid in presence of a negligible plastic behaviour (small scale yielding condition). In other words, the plastic zone must, for the case under analysis, be inside the zone at which the elastic stresses are being taken as a reference to predict the damage onset. This question has been already studied and will be addressed in a forthcoming publication.

6. Conclusions

A complete singular stress characterization has been carried out at the neighbourhood of the various multimaterial corners appearing in a typical metal-to-composite adhesively bonded double-lap joint by means of an asymptotic series expansion controlled by the GSIFs which are computed by means of a BEM model.

The results obtained from this singular stress analysis have been compared with those directly coming from a regular BEM analysis, a satisfactory agreement at a representative distance that validates the two procedures employed having been reached.

The study carried out has proved that only a 6% of the value of the total stress is due to non singular terms of the asymptotic series expansion, which leads to consider that the singular stress field is controlling the onset of the failure.

In order to analyze the representativity of such a characterization in the failure of the adhesive joints, a preliminary test program has been carried out. Different failure paths, corresponding to typical stacking sequences in the composite adherent, have been observed, all of them running through some of the multimaterial corners in the joint. This fact justifies the development of the tools for the asymptotic stress characterization from the previous works [21,22,25,33,34].

It can be deduced, from the good agreement observed between the predictions and experimental evidence regarding the failure angles, that all failure paths have been clearly influenced by the presence of the multimaterial corners appearing at these joints. This makes the singular stress characterization of these anisotropic multimaterial corners of major importance.

The capability of the tools developed for the characterization of the asymptotic stress state in these corners, together with the good numerical-experimental correlation found in the tests performed, open the possibility of using the parameters which define the singular stress state (GISF) in failure criteria proposals. It will require to design suitable specimens and to perform a large set of experiments on them to elucidate the role of singular field parameters on the onset of damage.

Acknowledgements

References

[1] Volkersen, O. "Die Nietkraftverteilung in Zugbeanspruchten mit Konstanten Laschenquerschnitten", *Luftfahrtforschung* (1938)*15: 41-47.*

[2] Goland, M. and Reissner, E. "The stresses in cemented joints", *Journal of Applied Mechanics* (1944) *11*: *A17-A27.*

[3] Hart-Smith, L. J., "Analysis and design of advanced composite bonded joints", *NASA CR-2218 (1974).*

[4] Tsai, M.Y., Oplinger, D.W. and Morton, J. "Improved theoretical solutions for adhesive lap joints", Int. J. of Solids and Structures (1998) 35: 1163-1185.

[5] Bogy, D.B. "Two edge bonded elastic wedges of different materials and wedge angles under surface tractions", Journal of Applied Mechanics (1971) 38: 377-386.

[6] Bogy, D.B. and Wang, K.C. "Stress singularities at interface corners in bonded dissimilar isotropic elastic materials", International Journal of Solids and Structures (1971) 7:993-1005.

[7] Groth, H. L. "Stress singularities and fracture at interface corners in bonded joints", *International Journal of Adhesion and Adhesives* (1988) *8*, *No. 2: 107-113.*

[8] Hattori, T. "A stress-singularity-parameter approach for evaluating the adhesive strength of single lap joints", *JSME Int. J. Series I,* (1991) *Vol. 34, No. 3: 326-331.*

[9] Leguillon, D. and Siruguet, K., "Finite fracture mechanics – application to the onset of a crack at a bimaterial corner". In: Karihaloo, B.L., (Ed.), Proceedings of the IUTAM Symp. on Analytical and Computational Fracture Mechanics of Non-Homogeneous Materials, Cardiff, UK, 18–22 June 2001. Kluwer Academic, Dordrecht, (2002): 11–18.

[10] D. Leguillon, J. Laurencin and M. Dupeux, "Failure initiation in an epoxy joint between two steel plates", *European J. of Mechanics* A/Solids (2003) 22: 509–524.

[11] Shin, K.C, Kim, W.S. and Lee, J.J. "Application of stress intensity to design of anisotropic/isotropic bi-materials with a wedge", *International Journal of Solids and Structures* (2007) 44: 7748–7766.

[12] Laschet, G. and Stas, A. "Finite element failure prediction of adhesive joints using a simple damage model", *Report SA-158*, *Université de Liège, Belgique* (1992).

[13] A. Sheppard, D. Kelly, L. Tong, "A damage zone model for the failure analysis of adhesively bonded joints", *Int. Journal of Adhesion and Adhesives*, (1998) 18: 385-400.

[14] Crocombe, A. D., "Global yielding as a failure criterion for bonded joints", *International Journal of Adhesion and Adhesives* (1989) 9: 145-153

[15] M.S. Kafkalidis, M.D. Thouless, "The effects of geometry and material properties on the fracture of single lap-shear joints", *International Journal of Solids and Structures* (2002) 39: 4367–4383.

[16] Liljedahl, C.D.M., Crocombe, A.D., Wahab, M.A. and Ashcroft, I.A., "Damage modelling of adhesively bonded joints", *Int. Journal of Fracture* (2006) 141: 147-161.

[17] Malyshev, B. M. and Salganik, R. L. "The strength of adhesive joints using the theory of cracks", *International Journal of Fracture* (1965) 1: 114-128.

[18] G. Fernlund, M. Papini, D. McCammond & J. K. Spelt, "Fracture load predictions for adhesive joints", *Composites Science and Technology* (1994) 51: 587-600.

[19] Reedy Jr., E.D., "Connection between interface corner and interfacial fracture analyses of an adhesively-bonded butt joint", *International Journal of Solids and Structures* (2000) 37: 2429-2442.

[20] Hutchinson, J.W. and Suo, Z. "Mixed mode cracking in layered materials" *Advances in Applied Mechanics*, Volume 29, (1992): 63-191.

[21] Barroso, A. "Characterization of singularity stress states in multimaterial corners. Application to adhesively bonded joints with composite materials", *Ph.D Thesis* (in Spanish), University of Seville (2007).

[22] Barroso A., Mantič, V. and París, F. "Singularity analysis of anisotropic multimaterial corners", *International Journal of Fracture* (2003) 119: 1-23.

[23] París, F. and Cañas, J. "*Boundary Element Method, Fundamentals and Applications*", Oxford University Press (1997).

[24] Graciani, E. "Formulation and implementation of the Boundary Element Method for axisymmetric contact problems. Application to fibre matrix interface characterization in composite materials", *Ph.D Thesis* (in Spanish), University of Seville (2006).

[25] Barroso A., Mantič, V. and París, F. "Evaluation of generalized stress intensity factors in anisotropic elastic multimaterial corners", European Conference on Composite Materials *ECCM-11* (2004), Rhodes, Greece, CD (paper Nº A032)

[26] Pageau, S. P., Gadi, K. S., Biggers, Jr., S. B. and Joseph, P. F. Standardized complex and logarithmic eigensolutions for n-material wedges and junctions, *International Journal of Fracture* (1996) 77: 51-76.

[27] ASTM D3528-96 (2002) Standard Test Method for Strength Properties of Double Lap Shear Adhesive Joints by Tension Loading.

[28] Wieghardt, K., "Über das Spalten und Zerreissen elasticher Körper," *Zeitschrift für Mathematik und Physi*k (1907) 55:60-103. English translation: "On splitting and cracking of elastic solids," *Fatigue Fracture Engng. Mater. Struct*. (1995) 18:1371-1405.

[29] Whitney, J.M. and Nuismer, R.J., "Stress fracture criteria for laminated composites containing stress concetrations," Journal of Composite Materials (1974) 8:253-265.

[30] Taylor, D., The Theory of Critical Distances A New Perspective in Fracture Mechanics, Elsevier, Amsterdam (2007).

[31] Leguillon, D., "Strength or toughness? A criterion for crack onset at a notch," *European Journal of Mechanics A/Solids* (2002) 21:61-72.

[32] Cornetti, P. Pugno, N., Carpinteri, A., Taylor, D., "Finite fracture mechanics: a coupled stress and energy failure criterion," *Engineering Fracture Mechanics* (2006) 73:2021-2033.

[33] Barroso, A., Mantič, V. and París, F. "Computing stress singularities in transversely isotropic multimaterial corners by means of explicit expressions of the orthonormalized Stroh-eigenvectors", Eng. Frac. Mech. (in press) doi:10.1016/j.engfracmech.2008.10.006

Comentado [P4]: aquí faltará o un punto o dos puntos

[34] Barroso, A., Mantič, V. and París, F. "Singularity parameter determination in adhesively bonded lap joints for use in failure criteria", *Composites Science and Technology* (2008) 68:2671-2677.